J Fusion Energ (2014) 33:32–39
DOI 10.1007/s10894-013-9636-7

ORIGINAL RESEARCH

Optimization of Fusion Pellet Launch Velocity in an Electrothermal Mass Accelerator

T. E. Gebhart · R. T. Holladay · M. J. Esmond · A. L. Winfrey

Published online: 1 October 2013

Abstract Electrothermal mass accelerators, based on capillary discharges, that form a plasma propelling force from the ablation of a low-z liner material are candidates for fuelling magnetic fusion reactors. As lithium is considered a fusion fuel and not an impurity, lithium hydride and lithium deuteride can serve as good ablating liners for plasma formation in an electrothermal plasma source to propel fusion pellets. A comprehensive study of solid lithium hydride and deuteride as liner materials to generate a plasma to propel cryogenic fuel pellets is presented here. This study was conducted using the ETFLOW capillary discharge code. Relationships between propellants, source and barrel geometry, pellet volume and aspect ratio, and pellet velocity are determined for pellets ranging in volume from 5 to 100 mm^3.

Keywords Fusion fuelling · Frozen pellets · Pellet aspect ratio · Capillary discharges · Electrothermal plasmas

T. E. Gebhart · R. T. Holladay · M. J. Esmond · A. L. Winfrey (✉)
Nuclear Engineering Program, Department of Mechanical Engineering, Virginia Polytechnic Institute and State University, Blacksburg, VA 24061-0238, USA
e-mail: leigh.winfrey@vt.edu

T. E. Gebhart
e-mail: tgebhart@vt.edu

R. T. Holladay
e-mail: rholla24@vt.edu

M. J. Esmond
e-mail: jemicah2@vt.edu

Introduction

Fueling of future tokamak reactors requires both deep and shallow pellet injection as a primary mechanism by which the burning plasma core is fueled. This is accomplished through fast injection of frozen deuterium or deuterium–tritium frozen pellets with velocities, on the order of 1–5 km/s, based on fueling needs [1, 2]. The velocities up to 3 km/s have already been shown to be an efficient technique to raise the plasma density in tokamaks [2]. There have been several studies on the pellet injection systems from the mid 1970's and researchers continue to investigate system improvements and technique enhancements [3–9]. Concepts and experiments on the use of light gas guns, pneumatic guns and electrothermal plasma sources have shown successful pellet injection at speeds sufficient for fueling tokamaks, however, electrothermal plasma guns have shown the capability to launch pellets at speeds in excess of 3 and 4 km/s [5, 7–9]. This computational study of a pellet acceleration system using an electrothermal (ET) mass accelerator addresses a wide range of system geometries and pellet characteristics for fueling and stability control of a tokamak fusion reactor, and explores how the geometric aspects of the ET injection system affect the exit velocities and firing rates of the pellets. It has been previously shown that this type of injection system provides a highly controllable and reproducible, low-Z mass accelerator suitable for fueling and stability control [8, 10, 11]. Additionally, the ET injection technique can be used to provide a range of exit velocities and pellet volumes that are suitable for both fueling and edge localized mode (ELM) mitigation requirements as dictated by tokamak design.

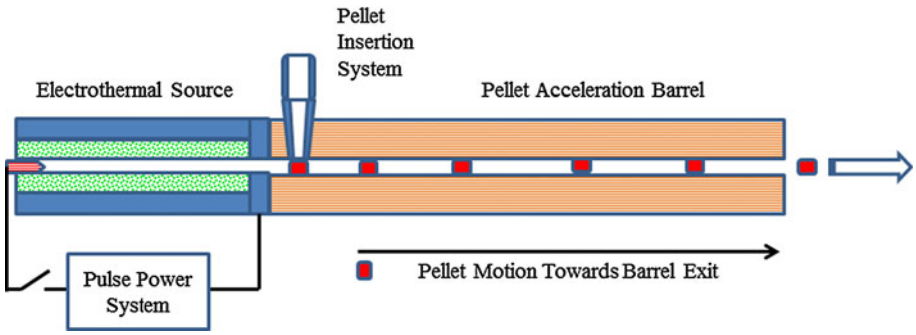

Fig. 1 Schematics of the electrothermal source and the barrel for acceleration of frozen pellets

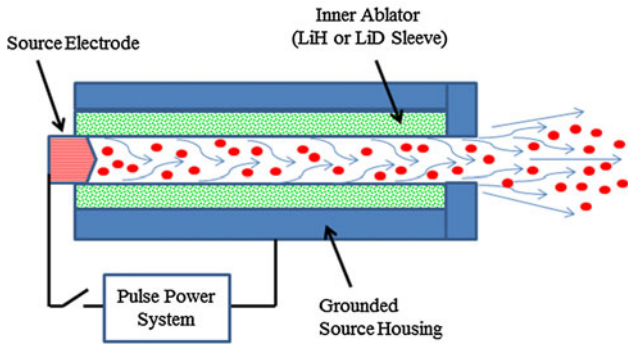

Fig. 2 Schematic of an electrothermal plasma source showing the plasma formation and flow

Electrothermal Capillary Pellet Launcher

Electrothermal (ET) plasma systems have numerous applications such as artillery propellants [12, 13], thrusters for spacecraft or satellite applications [14–16], hypervelocity launchers [17–19], and high heat flux sources for materials studies [20, 21]. An illustration of an electrothermal (ET) plasma pellet accelerator is shown in Fig. 1, where the electrothermal source is a low-Z liner such as lithium hydride (LiH) or lithium deuteride (LiD). A pulsed power system is connected to an electrode that is inserted into the capillary. As the current is discharged, it causes the low-Z liner to ablate due to the radiative heat flux on the inner wall of the liner material. The ablated material becomes ionized and flows out of the source with very a high momentum and a high pressure value is reached at the source exit.

The source is connected to a barrel; the cryogenically frozen deuterium–tritium pellet that has been compressed into the pellet chamber resides at the interface between the source exit and the barrel inlet. The pellet is formulated from deuterium and tritium supplied from a main gas delivery system equipped with freezing, extrusion, slicing and loading capabilities into the interface between the source and the barrel. These methods are similar to the techniques proposed by other researchers [6, 8, 22–24]. The driving force is the plasma generated from the ablation of the source liner, which results from the high heat flux radiated from the discharge arc. The source liner ablates to form a dense plasma with high pressure and high flow speed, as illustrated in Fig. 2.

The computational study discussed here was conducted using the ETFLOW code [25], which is a 1-D, time-dependent, electrothermal plasma code with ideal and nonideal plasma conductivity model that simulate plasma generation and flow through the capillary source. ETFLOW also calculates the internal ballistics of a projectile's path through a barrel attached to the source, accounting for variables such as pellet release pressure and friction losses. The simulations that were carried out for this study were performed using the ideal conductivity model, details of these models are discussed elsewhere [25].

The source section model in ETFLOW has three basic governing equations, conservation of mass, momentum, and energy. The model is based on that of Hurley et al. [26], which included wall ablation and introduced the ablation rate into the governing equations, and the subsequent modifications by Kincaid et al. [5, 27] to account for the addition of the motion of the pellet into the extension barrel, its momentum, friction and kinetic energy. The governing equations for the extension barrel are identical to the equations of the source except that the joule heating term is removed from the energy equation as there is no electric current discharge in the barrel section. The ETFLOW code is the newest version of the ET plasma code written in FORTRAN that runs in the VBA environment with additional modules such as materials libraries, pulse power generators, plasma conductivity modules, and switches to run with or without axial heat conduction or magnetic pressure. A detailed description of the model physics and the ETFLOW code are given elsewhere [8, 25]. The code was validated by experiments conducted by Winfrey et al. [25] and has shown that the experimental values fell in between the code results for the ideal and non-ideal conductivity models.

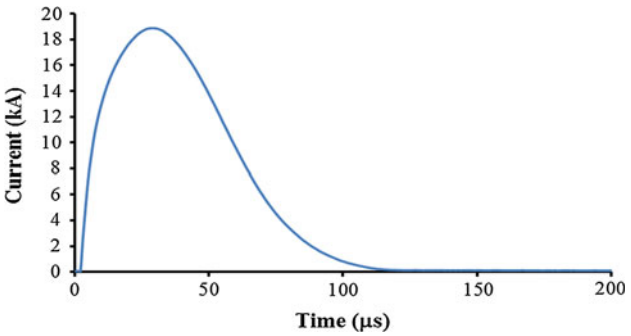

Fig. 3 Plot of the discharge current of 19 kA peak and 100 μs pulse length

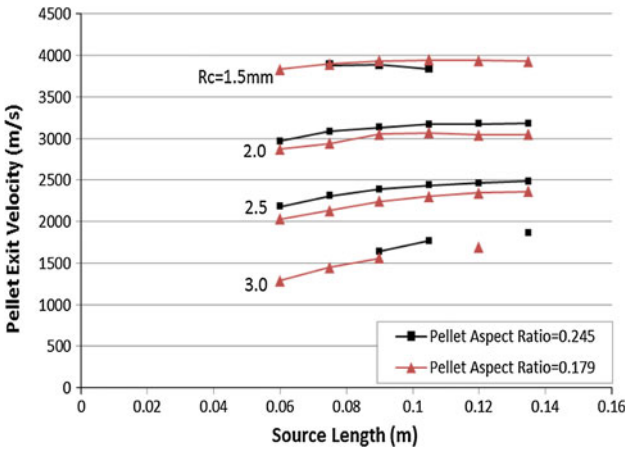

Fig. 4 Pellet exit velocities with respect to different source sizes and pellet aspect ratios

Simulation Parameters

A study was conducted using a discharge current that peaked at approximately 19 kA with an active pulse time of approximately 100 μs as shown in Fig. 3. A series of ET-FLOW code runs were conducted for two separate source sizes; 10 cm in length by 2.5 mm radius and 9 cm in length by 1.5 mm radius. For each source size, barrel radii of 2, 2.25, 2.5, 2.75, and 3 mm were explored. This range of barrel radii was chosen to see how small changes affect the pellet outcomes. For each barrel radius, pellet volumes of 5, 10, 20, 35, 50, 60, 75, 90, and 100 mm^3 were examined, and for each pellet volume, barrel lengths of 0.1, 0.2, 0.3, and 0.4 m were investigated. All runs were conducted with a LiD source liner as the ablative material and a steel barrel as the acceleration section. Other studies have shown that of low-Z materials that were tested, LiD produced a higher velocity per unit of input energy [7, 8].

An initial set of runs was conducted in order to examine the effects of varying the source size on pellet exit velocity to determine which source sizes should be further explored. Figure 4 shows a plot of the exit velocity for different source sizes for two different aspect ratios of 20 mm^3 pellets. All of these runs were conducted with a 0.2 m barrel length, along with the same materials and shot characteristics discussed above. In the legend of the plot, PS-1 and PS-2 refer to the two different pellet aspect ratios, and RC is the radius of the capillary. These data suggest exploring multiple source sizes is of value due to the broad range of exit parameters achieved. A capillary with a length of 10 cm and a radius of 2.5 mm was chosen because it produced an average range of exit velocities. The second chosen source size is one with length of 9 cm and a radius of 1.5 mm because it produced higher velocities, but not so high that pellet cracking or large particle collision losses would occur. Exploring the different source aspect ratios is a starting point for any further work on this topic. The source size plays an essential role in the exit velocity of the pellets as shown in Fig. 4.

Effect of Pellet Size on Exit Velocity

A plot of pellet exit velocity versus pellet aspect ratio is shown in Fig. 5. This is plot includes both source sizes as is seen in the two distinct curve groups shown. After the exit velocity peaks on both curves, it is apparent that as the aspect ratio increases, the velocity will approach a certain characteristic speed. The data plotted in Fig. 5 shows data for all barrel lengths, both source sizes, and all pellet volumes.

The range of velocities for the larger source size, 10 cm length by 2.5 mm radius, was between 990 and 2,660 m/s with a characteristic velocity of approximately 2,500 m/s. The smaller source size, 9 cm in length by 1.5 mm radius, had a velocity range between 1,946 and 4,045 m/s with a characteristic velocity of approximately 3,600 m/s. In examining the trend of the data in Fig. 5, it can be noted that a slight change in the pellet's aspect ratio leads to a large change in the exit velocity when the aspect ratio is less than 2. As aspect ratios increase above 2, the velocity is less and less affected by the change. This trend is evident for both source sizes. As the barrel length increases for the larger source, the velocities decrease in a quadratic fashion. This is because the pressure does not build up as much as it does in the smaller source due to the increased friction drag. The larger barrel lengths for the smaller source have higher exit velocities because of the ability to build up pressure and propel the pellet with more energy.

In order to remove pellet volume and barrel length as parameters that could affect exit velocity, Figs. 6, 7 were generated for constant pellet volume and barrel length. Figure 6 shows the exit velocities for a volume of 50 mm^3 and a barrel length of 0.2 m. Figure 7 also shows the exit velocities for a barrel length of 0.2 m, except for a volume

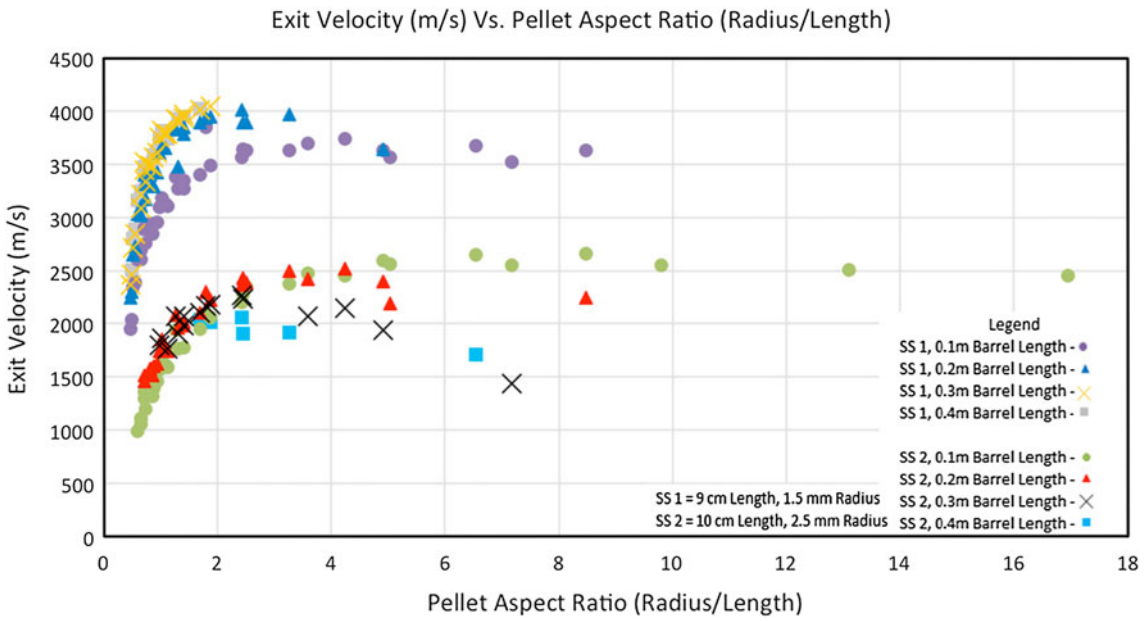

Fig. 5 Pellet aspect ratio versus exit velocity for all barrel lengths, both source sizes, and all pellet volumes

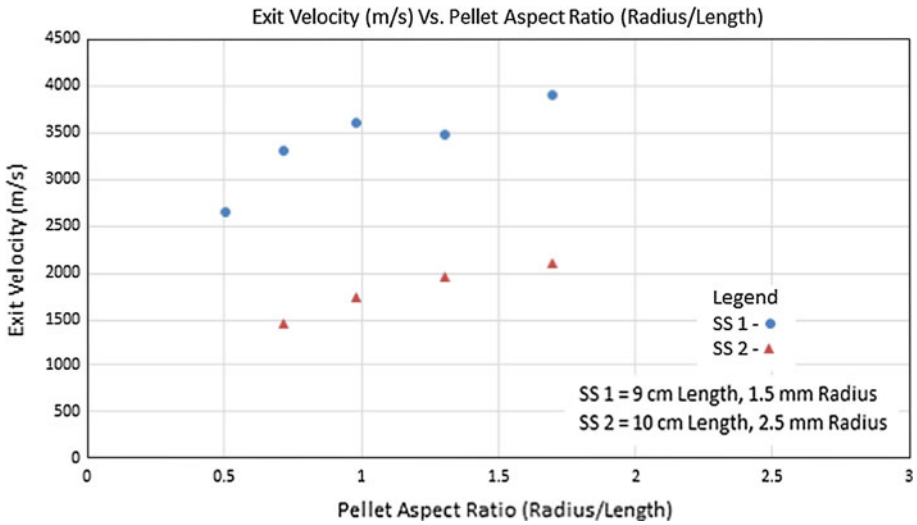

Fig. 6 Pellet exit velocity versus pellet's aspect ratio for a barrel length of 0.2 m and a constant volume of 50 mm^3

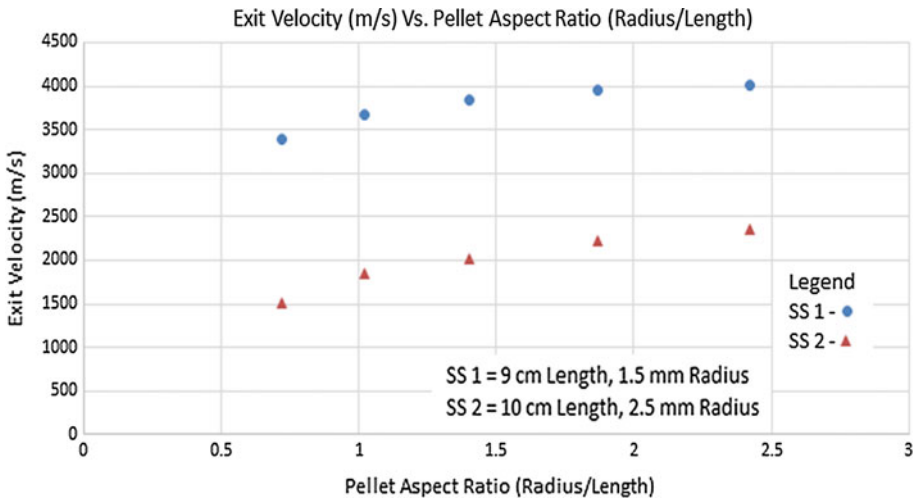

Fig. 7 Pellet exit velocity versus pellet's aspect ratio for a constant volume of 35 mm^3 and a barrel length of 0.2 m

of 35 mm^3. This allows for a more specific analysis of how the pellet aspect ratio impacts exit velocity.

From Figs. 6, 7, it can be seen that isovolumetric pellets will have different exit velocities based on source geometry and aspect ratio. Looking at either source size, a specific amount of material, i.e. volume, may be delivered at any necessary velocity by changing the launcher geometry and pellet aspect ratio. Comparing the range of aspect ratios between pellet volumes of 35 and 50 mm^3, it can be seen that as the pellet volumes become larger, their pellet aspect ratios become smaller because the pellet lengths increase as the radius of the barrel and pellet remain constant. The general trend of exit velocity to aspect ratio for each pellet volume, seen in Figs. 6, 7, follows the larger trend, shown in Fig. 5, that a characteristic velocity is approached at higher aspect ratios.

The general trend of exit velocity to aspect ratio for each pellet volume, seen in Figs. 6, 7, follows the larger trend, shown in Fig. 5, that a characteristic velocity is approached at higher aspect ratios. To further the exploration of pellet size on exit velocities, the pellet radius was taken out of the analysis since it is constant. Figure 8 shows the slightly

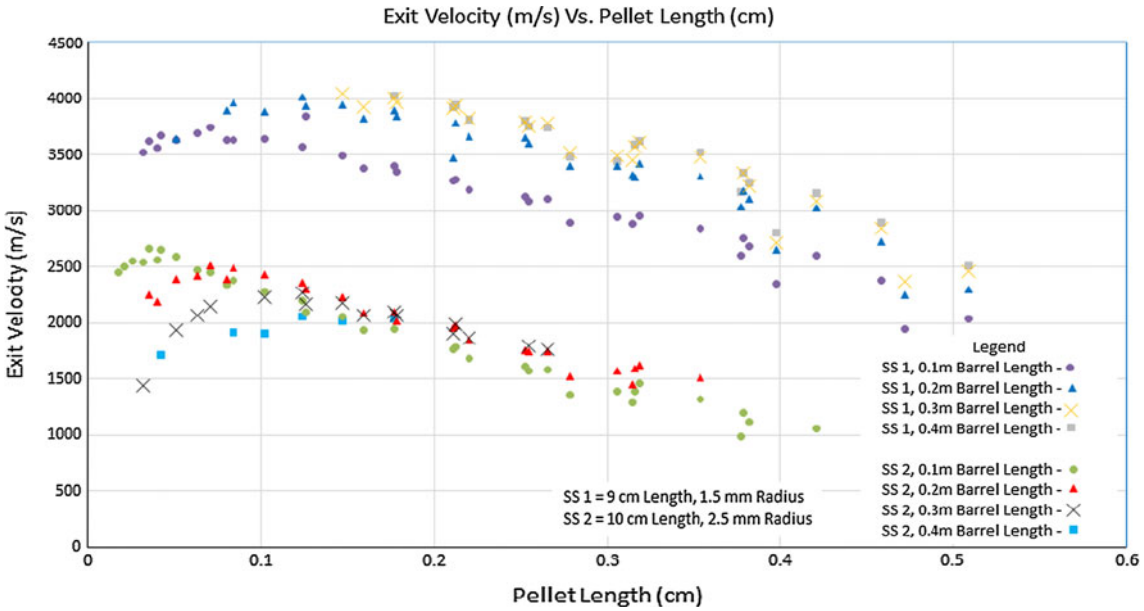

Fig. 8 Pellet exit velocity versus pellet's length to illustrate the relationship of the system without barrel/pellet radius

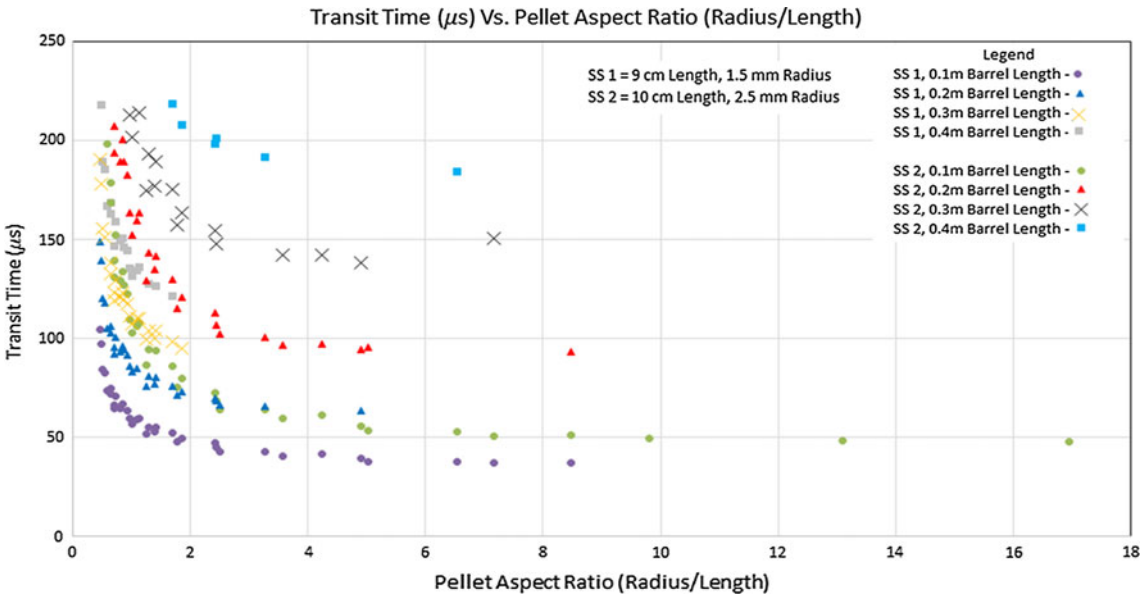

Fig. 9 Transit time versus pellet aspect ratio showing trends corresponding to the ability to reach a certain shot frequency

quadratic relationship between and exit velocity and pellet length. This relationship further demonstrates the range of velocities that this ET plasma mass acceleration system can achieve.

Effect of Pellet Size on Pellet Transit Time

The transit time is defined as the time the pellet starts moving through the barrel until the time when it leaves the barrel. In all cases, the pellet starts moving between 8 and 30 μs after the discharge current is initiated. Figure 9 shows a plot of the transit time and the pellet's aspect ratio. For each source size, there are four distinct lines that correspond to each barrel length, 0.1, 0.2, 0.3, and 0.4 m. The difference in these lines is due to increased transit times for longer barrels. The general trend shows that as the pellet aspect ratio decreases, the transit time will increase. The shorter the barrel, the less time it will take the pellet to move through it.

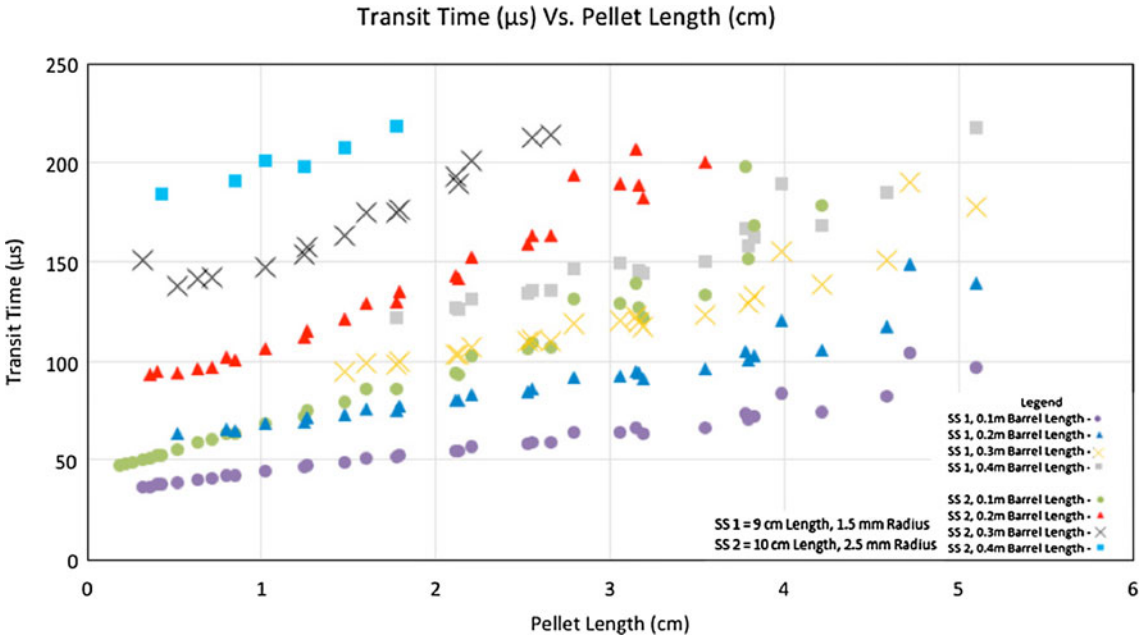

Fig. 10 Pellet transit time versus pellet length

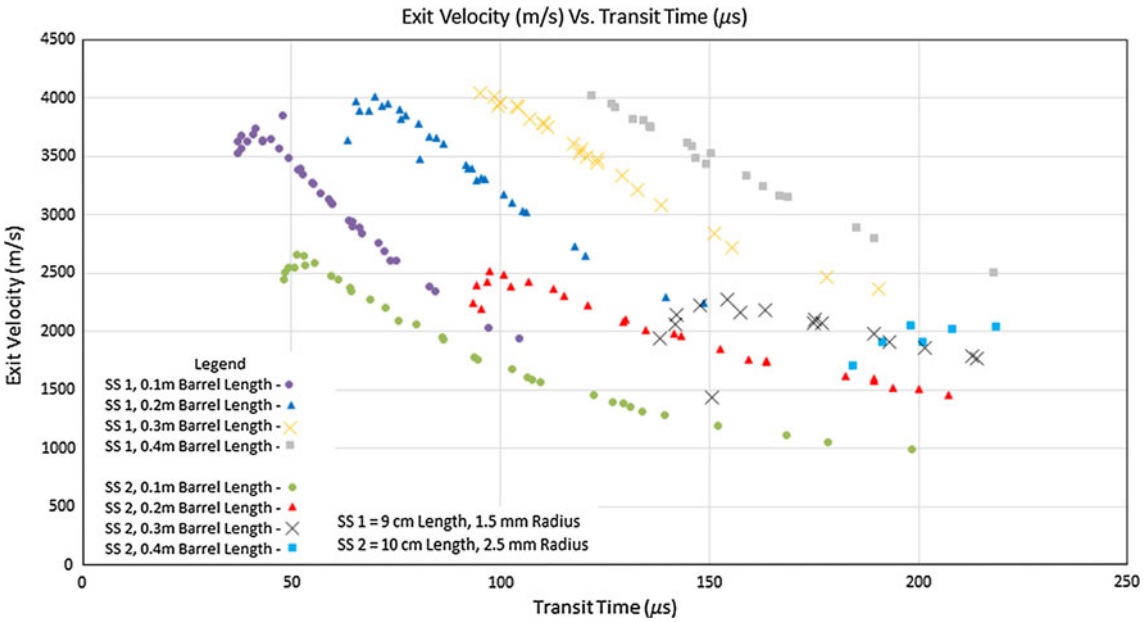

Fig. 11 Pellet exit velocity versus transit time showing the overall trends corresponding to shot frequency and exit speeds

Figure 10 shows the transit time versus pellet length. As barrel and pellet radius is removed from the plot, a mostly linear relationship appears for each barrel length. As pellet length increases, the transit time increases. Again, there are four distinct data trends for each of the source sizes, one for each barrel length for each simulation run.

The capability for variable transit time will allow the fuel injection system to be more versatile to the tokamak fueling needs. Fueling and ELM mitigation shots will need to be fired at different frequencies. Launches with a large pellet transit time cannot be set to fire at a high frequency, whereas launches with low transit times can be fired in faster succession. The range of transit times produced by these two source sizes covers a broad range that easily includes fueling and ELM mitigation shot frequencies. To further demonstrate the versatility of this system with respect to the shot frequency, a series of larger barrel radii should be explored in order to increase the aspect ratios to find a point where the transit times decrease enough for any necessary task, however, increased barrel radii will require the use of a 2-D version of ETFLOW, which is under development as a semi-2-D code [28–30].

Relationship of Exit Velocity and Pellet Transit Time

Figure 11 illustrates the pellet's exit velocity versus its transit time. This figure ties together the whole range of possibilities of the ET pellet launching system. The basic trend here shows that as the transit time increases, the velocity decreases. This is due to the friction drag in the longer barrels. As with the previous plots, there are four distinct sets of data for each of the two source sizes. This is again due to the four different barrel lengths that were explored. At the tops of each 0.1 and 0.2 m barrel lines, there is a roll-over. This roll-over is due to the fact that the pressure behind the pellet does not build up to its maximum before the pellet leaves the barrel, so energy is wasted. Avoiding wasted energy could be achieved by using a lower power shot or by using an optimal barrel length.

Conclusions

Based on the previously described data, the system is fully capable of reaching the necessary specifications for any type of pellet injection into magnetically confined plasma for both ELM mitigation and fueling. The following relationships were discovered: as the pellet aspect ratio rises, the exit velocity rises sharply until an aspect ratio of approximately 2 is reached. Once an aspect ratio of 2 is reached, the pellet velocity levels off at a value characteristic to the size of the source. Removing the pellet radius from the aspect ratio, the relationship between pellet length and exit velocity was found to be linear for aspect ratios less than 1. As the pellet length decreases, the exit velocity increases because of the decreased kinetic friction drag of the pellet in the barrel. Besides pellet velocity, transit time was also explored in order to show that the transit times would not interfere with the shot frequency. Even with the longest barrel and pellet, the highest transit time was approximately 220 μs, which translates to a shot frequency of over 4,000 shots per second, which means that the electrical supply will be the limiting factor in shot frequency. The transit time was plotted against exit velocity, showing that as the pellets get larger, they take longer to transmit through the barrel. More code runs are needed in order to further the validation of the versatility of the ET pellet injection system. Exploration of varied discharge amplitudes along with smaller and larger source sizes is necessary.

Acknowledgments Work supported by the Virginia Tech Nuclear Engineering Program. The authors thank Dr. M.A. Bourham at N.C. State University for his generosity in sharing his time and insight in discussions and comments.

References

1. D. Babineau, S. Maruyama, R. Pearce, M. Glugla, Li Bo, B. Rogers, S. Willms, G. Piazza, T. Yamanishi, S. H. Yun, L. Worth, W. Shu, Review of the ITER fuel cycle. In *Proceedings of 23rd IAEA Fusion Energy Conference*, 11–16 October, Daejeon, Republic of Korea, paper ITR2/2 (2010)
2. D. Frigione, L. Garzotti, C.D. Challis, M. De Baar, P. De Vries, M. Brix, X. Garbet, N. Hawkes, A. Thyagaraja, L. Zabeo, JET EFDA contributors, Pellet injection and high density ITB formation in JET advanced tokamak Plasmas. EFDA–JET–PR(06)13. In *Proceedings of 20th IAEA Fusion Energy Conference*, Vilamoura, Portugal, pp. 1–22 (2004)
3. S.L. Milora, C.A. Foster, Pneumatic hydrogen pellet injection system for the ISX tokamak. Rev. Sci. Instrum. **50**(4), 482 (1979)
4. S.K. Combs, C.R. Foust, S.L. Milora, Small-bore (1.8 mm), high-firing-rate (10 Hz) version of a repeating pneumatic hydrogen pellet injector. Rev. Sci. Instrum. **33**, 2736 (1995)
5. R.W. Kincaid, M.A. Bourham, Plasma gun pellet acceleration modeling and experiment. Fusion Technol. **30**, 834 (1996)
6. S.J. Meitner, L.R. Baylor, S.K. Combs, D.T. Fehling, J.M. McGill, D.A. Rasmussen, J.W. Leachman, Development of a twin-screw D2 extruder for the ITER pellet injection system. Fusion Sci. Technol. **56**, 52 (2009)
7. A.L. Winfrey, M.A. Abd Al-Halim, J.G. Gilligan, A.V. Saveliev, M.A. Bourham, Modeling of an ablation-free electrothermal plasma pellet accelerator. Fusion Sci. Technol. **60**, 480 (2011)
8. A.L. Winfrey, J.G. Gilligan, M.A. Bourham, A computational study of a capillary discharge pellet accelerator concept for magnetic fusion fueling. J. Fusion Energ **32**, 227 (2012)
9. A.L. Winfrey, M.A. Abd Al-Halim, A.V. Saveliev, J.G. Gilligan, M.A. Bourham, Enhanced performance of electrothermal plasma sources as fusion pellet injection drivers and space based mini-thrusters via extension of a flattop discharge current. J. Fusion Energ **32**, 371 (2013)

10. L.R. Baylor, T.C. Jernigan, R.J. Colchin, Characteristics of ELM activity and fueling efficiency of pellet injection from different locations on DIII-D. J. Nuclear Mater **290–293**, 398 (2001)
11. L.R. Baylor, T.C. Jernigan, C. Hsieh, Deposition of fuel pellets injected into tokamak plasmas. Fusion Technol. **34**(3), 425 (1998)
12. R. Alimi, L. Bakshi, E. Kot, Experimental ballistic improvement in a pure electrothermal 25-mm gun. IEEE Trans. Magn. **43**(1), 284 (2007)
13. R. Alimi, L. Bakshi, E. Kot, Temperature compensation and improved ballistic performance in a solid-propellant electrothremal-chemical 40-mm gun. IEEE Trans. Magn. **43**(1), 289 (2007)
14. S.Y. Wang, P.J. Staiger, *Primary Propulsion of Electrothermal, Ion, and Chemical Systems for Space-Based Radar Orbit Transfer*. NASA technical memorandum 87043, NAS 1.15:87043 (1985)
15. T. Edamitsu, H. Tahara, Experimental and numerical study of an electrothermal pulsed plasma thruster for small satellites. Vacuum **80**, 1223 (2006)
16. Y. Takao, K. Eriguchi, K. Ono, A miniature electrothermal thruster using microwave-excited microplasmas: thrust measurement and its comparison with numerical analysis. J. Appl. Phys. **101**, 123307 (2007)
17. F.D. Witherspoon, R.L. Burton, S.A. Goldstein, A second generation EMET railgun for secondary arc studies. IEEE Trans. Magn. **27**, 91 (1991)
18. J. Dyvik, J. Herbig, R. Appleton, J. O'Reilly, J. Shin, Recent activities in electro-thermal chemical launcher technologies at BAE systems. In *13th International Symposium on Electromagnetic Launch Technology (EML)*, May 22–25, Potsdam, Brandenburg, Germany (2006)
19. C.M. Edwards, M.A. Bourham, J.G. Gilligan, Experimental studies of the plasma-propellant interface for electrothermal-chemical launchers. IEEE Trans. Magn. **31**, 404 (1995)
20. J.G. Gilligan, M.A. Bourham, The use of an electrothermal plasma gun to simulate the extremely high heat flux conditions of a tokamak disruption. J. Fusion Energ **12**, 311 (1993)
21. J.P. Sharpe, M.A. Bourham, J.G. Gilligan, Generation and characterization of carbon particulate in disruption simulations. Fusion Technol. **34**, 634 (1998)
22. S.K. Combs, M.J. Gouge, L.R. Baylor, Development of pellet injection systems for ITER. In *Proceedings of IEEE Symposium of Fusion Energy* (1995 SOFE, Sept 30–Oct 5), Champaign, IL, USA, 1607 (1995)
23. B.V. Kuteev, A.P. Umov, I.V. Viniar, Pellet injection research and development program. Plasma Devices Oper. **2**, 193 (1994)
24. M.J. Gouge, K.D. St. Onnge, S.L. Milora, Pellet fueling systems for ITER. Fusion Eng. Des. **19**, 53 (1992)
25. A.L. Winfrey, M.A. Bourham, J.G. Gilligan, A study of plasma parameters in a capillary discharge with calculations using ideal and nonideal plasma models for comparison with experiment. IEEE Trans. Plasma Sci. **40**, 843 (2012)
26. J.D. Hurley, M.A. Bourham, J.G. Gilligan, Numerical simulations and experiment of plasma flow in the electrothermal launcher SIRENS. IEEE Trans. Plasma Sci. **31**, 616 (1995)
27. R.W. Kincaid, M.A. Bourham, J. G. Gilligan, acceleration using an ablation-controlled electrothermal launcher. In *Proceedings of IEEE Symposium of Fusion Energy* (1995 SOFE, Sept 30–Oct 5), Champaign, IL, USA, 1613 (1995)
28. H. Ngo, *A Pseudo Two-Dimensional Time-Dependent Model of the Heat and Current Transport Within an Electrothermal Plasma Source*. MNE Thesis, North Carolina State University, 1998
29. B. Lamber, *Effect of Incorporation of a New Model for Electron-Ion Collision Frequency in an Electrothermal Plasma Launcher*. MNE Thesis, North Carolina State University, 2000
30. A.L. Winfrey, *A Numerical Study of the Non-ideal Behavior, Parameters, and Novel Applications of an Electrothermal Plasma Source*. PhD Dissertation, North Carolina State University, 2010